Topoisomerase 1 Inhibition in MYC-Driven Cancer Promotes Aberrant R-Loop Accumulation to Induce Synthetic Lethality

Peter Lin[1,2], Corey Lourenco[1,2], Jennifer Cruickshank[2], Luis Palomero[3], Jenna E. van Leeuwen[1,2], Amy H. Y. Tong[4], Katherine Chan[4], Samah El Ghamrasni[2], Miquel Angel Pujana[3,5], David W. Cescon[2,6], Jason Moffat[4,7,8,9], and Linda Z. Penn[1,2]

ABSTRACT

MYC is a central regulator of gene transcription and is frequently dysregulated in human cancers. As targeting MYC directly is challenging, an alternative strategy is to identify specific proteins or processes required for MYC to function as a potent cancer driver that can be targeted to result in synthetic lethality. To identify potential targets in MYC-driven cancers, we performed a genome-wide CRISPR knockout screen using an isogenic pair of breast cancer cell lines in which MYC dysregulation is the switch from benign to transformed tumor growth. Proteins that regulate R-loops were identified as a potential class of synthetic lethal targets. Dysregulated MYC elevated global transcription and coincident R-loop accumulation. Topoisomerase 1 (TOP1), a regulator of R-loops by DNA topology, was validated to be a vulnerability in cells with high MYC activity. Genetic knockdown of TOP1 in MYC-transformed cells resulted in reduced colony formation compared with control cells, demonstrating synthetic lethality. Overexpression of RNaseH1, a riboendonuclease that specifically degrades R-loops, rescued the reduction in clonogenicity induced by TOP1 deficiency, demonstrating that this vulnerability is driven by aberrant R-loop accumulation. Genetic and pharmacologic TOP1 inhibition selectively reduced the fitness of MYC-transformed tumors *in vivo*. Finally, drug response to TOP1 inhibitors (i.e., topotecan) significantly correlated with MYC levels and activity across panels of breast cancer cell lines and patient-derived organoids. Together, these results highlight TOP1 as a promising target for MYC-driven cancers.

Significance: CRISPR screening reveals topoisomerase 1 as an immediately actionable vulnerability in cancers harboring MYC as a driver oncoprotein that can be targeted with clinically approved inhibitors.

Introduction

The c-MYC (MYC) oncoprotein is dysregulated in most human cancers. MYC is a master regulator of gene transcription that controls numerous biological processes, and when dysregulated, drives many hallmarks of cancer (1). Inhibition of MYC in mouse models blocks tumor growth, demonstrating that the development of MYC inhibitors may improve cancer patient outcomes (2). However, small molecules that directly inhibit MYC have not advanced to patient care.

Synthetic-lethal vulnerabilities in MYC-dysregulated tumors (MYC-SL) describe a state in which MYC-transformed cancer cells depend on specific proteins or processes to maintain viability (3). Exploiting these MYC-driven vulnerabilities is a promising approach for indirectly targeting MYC in cancer. To identify MYC-SLs, genetic screens have been performed in models where MYC is dysregulated but is not necessarily the driver oncogene that initiates and sustains normal-to-tumor cellular transformation (4–11). We recently developed a MYC-driven and -dependent model of human breast cancer (10A.PM) and an isogenic control (10A.PE; ref. 12). When introduced into mice, 10A.PM cells produce invasive ductal carcinomas that model human disease at the histological and molecular levels, whereas 10A.PE cells develop benign acinar structures.

To identify MYC-SLs, we conducted a genome-wide CRISPR knockout screen using the 10A.PE and 10A.PM isogenic pair. We identified many R-loop factors that were differentially required for the survival of 10A.PM but not 10A.PE cells. R-loops are three-stranded nucleic acid structures that include a DNA:RNA hybrid and a displaced single-stranded DNA. The regulation of R-loops is dynamic; however, if pathologic R-loops remain unresolved, they can contribute to DNA damage and genomic instability (13). Importantly, R-loop factors such as ribonucleases, helicases, and topoisomerases regulate R-loop accumulation (13). We prioritized the validation of TOP1 as a novel MYC-SL vulnerability because FDA-approved TOP1 inhibitors (i.e., topotecan, irinotecan) were immediately available, and TOP1 inhibitor antibody drug conjugates (TOP1-ADC) have recently emerged as standard and highly effective therapies for breast cancer (14). Genetic and pharmacologic inhibition of TOP1 was demonstrated to be synthetic-lethal in MYC-dysregulated breast cancer cells and inhibited tumor growth *in vivo*. We identified an association between MYC target gene signature enrichment and TOP1 inhibitor

[1]Department of Medical Biophysics, University of Toronto, Toronto, Canada. [2]Princess Margaret Cancer Centre, University Health Network, Toronto, Canada. [3]ProCURE, Catalan Institute of Oncology, Oncobell, Bellvitge Institute for Biomedical Research (IDIBELL), L'Hospitalet del Llobregat, Barcelona, Spain. [4]Donnelly Centre, University of Toronto, Toronto, Canada. [5]CIBERES, Instituto de Salud Carlos III, Madrid, Spain. [6]Division of Medical Oncology and Hematology, Department of Medicine, University of Toronto, Toronto, Canada. [7]Genetics and Genome Biology, The Hospital for Sick Children, Toronto, Canada. [8]Department of Molecular Genetics, University of Toronto, Toronto, Canada. [9]Institute for Biomedical Engineering, University of Toronto, Toronto, Canada.

P. Lin and C. Lourenco contributed equally to this article.

Corresponding Author: Linda Z. Penn, Genomics and Epigenetics Program, Princess Margaret Cancer Centre, 13th Floor 13-706, Toronto, Ontario, M5G 1L7, Canada. E-mail: Linda.Penn@uhnresearch.ca

Cancer Res 2023;XX:XX–XX

doi: 10.1158/0008-5472.CAN-22-2948

drug response in cancer cells using publicly available datasets. Finally, TOP1 inhibitor drug response was then shown to be significantly correlated with MYC levels and activity in a panel of breast cancer cell lines and patient-derived organoids. Taken together, this work reveals an opportunity to exploit TOP1 as a vulnerability in MYC-driven cancers and use MYC activity as a potential biomarker for TOP1-directed therapies.

Materials and Methods

Cell culture

MCF10A mammary epithelial cells were a kind gift of Dr. Senthil Muthuswamy (NIH) and were cultured in DMEM/F12 (Wisent; catalog no. 319–075-CL) supplemented with 5% horse serum (Thermo Fisher Scientific; catalog no. 16050114), 20 ng/mL epidermal growth factor (Peprotech; catalog no. AF-100–15), 100 ng/mL hydrocortisone (Sigma; catalog no. H0888–5G), 100 ng/mL cholera toxin (Sigma; C8052–2MG), 10 μg/mL insulin (Sigma; catalog no. I9278–5ML) and 100 U/mL penicillin/streptomycin (Thermo Fisher Scientific; catalog no. 15140122). The generation of 10A.PE and 10A.PM cells from MCF10A cells was performed as described previously (12). Inducible expression of empty vector or MYC in 10A.PE and 10A.PM cells, respectively, was performed by culturing cells in 2 μg/mL doxycycline (Sigma-Aldrich; catalog no. D9891–25G) for 24 hours. P493–6 cells were a kind gift from Dr. Chi Van Dang (John Hopkins University). The HCC1806, SKBR3, and MDA-MB-231 cell lines were kind gifts from the late Dr. Mona Gauthier (Princess Margaret Cancer Centre). MCF7 cells were a kind gift from Dr. Amadeo Parissenti (Northeast Cancer Centre). The SUM159PT, Hs578t, and MDA-MB-436 cell lines were kind gifts from Dr. Benjamin Neel (University Health Network). The MDA-MB-175VII and the HCC70 cell lines were kind gifts from Dr. David Cescon (Princess Margaret Cancer Centre). P493–6 cells were cultured in RPMI1640 (Wisent; catalog no. 350–000-CL) supplemented with 10% FBS (Wisent; catalog no. 080–150) and 100 U/mL penicillin/streptomycin. HCC1806 and HCC70 cells were cultured in RPMI1640 with 10% FBS and 100 U/mL penicillin/streptomycin. MDA-MB-231, MDA-MB-175VII, Hs578t, and MCF7 cells were cultured in DMEM (Wisent; catalog no. 319–005-CL) with 10% FBS and 100 U/mL penicillin/streptomycin. MDA-MB-436 cells were cultured in DMEM with 10% FBS, 10 μg/mL insulin, and 100 U/mL penicillin/streptomycin. SKBR3 cells were cultured in McCoy's 5A (Thermo Fisher Scientific; catalog no. 16600082) with 10% FBS and 100 U/mL penicillin/streptomycin. SUM159PT cells were cultured in Ham's F12 (Thermo Fisher Scientific; catalog no. 11765054) with 5% FBS, 5 μg/mL insulin, 1 μg/mL hydrocortisone, 10 mmol/L HEPES, and 100 U/mL penicillin/streptomycin. All cell lines were cultured in a humidified incubator at 37°C in the presence of 5% CO_2 and 95% air. The authenticity of cell lines were validated by short-tandem repeat profiling at The Centre for Applied Genomics and were routinely monitored for *Mycoplasma* contamination (Lonza MycoAlert Mycoplasma Detection Kit; catalog no. LT07–118). Cell lines were used for 5 to 10 passages from the initial expansion and freeze-down.

Lentiviral transfection and transduction

HEK293Tv cells were a kind gift of Dr. Sam Benchimol and were transfected with lentiviral DNA constructs and packaging plasmids pMD2.G (RRID:Addgene_12259) and psPAX2 (RRID:Addgene_12260) via calcium phosphate precipitation. Approximately 72 hours after transfection, viral supernatants were harvested and filtered in 0.45 μm syringe filters prior to storage at −80°C. For transduction, cells were infected with lentivirus in 0.8 mg/mL polybrene for approximately 24 hours prior to selection with puromycin (BioShop; catalog no. PUR333.100), blasticidin (BioShop; catalog no. BLA477.50), Geneticin (Thermo Fisher Scientific; catalog no. 10131035), or hygromycin B (BioShop; catalog no. HYG002.1).

Lentiviral short-hairpin RNA

Short-hairpin RNA targeting sequences were designed using the Genetic Perturbation Platform (Broad Institute; https://portals.broadinstitute.org/gpp/public/gene/search). For each shRNA, forward and reverse oligos were annealed and cloned into Tet-pLKO-puro (a gift from Dmitri Wiederschain; RRID:Addgene_21915) for lentiviral production and subsequent transduction into destination cell lines. Negative control shRNAs (shCTRL) targeting LacZ were used. shTOP1–1 was designed to target the coding sequence of the *TOP1* gene, whereas shTOP1–2 was designed to target the 3′ UTR:

TOP1–1 Forward:
5′CCGGCATAGCAACAGTGAACATAAACTCGAGTTTATGTTCACTGTTGCTATGTTTT TG 3′

TOP1–1 Reverse:
5′AATTCAAAAACATAGCAACAGTGAACATAAACTCGAGTTTATGTTCACTGTTGCTA TG 3′

TOP1–2 Forward:
5′CCGGTGAAGGGCGAGTGAATCTAAGCTCGAGCTTAGATTCACTCGCCCTTCATTTT TG 3′

TOP1–2 Reverse:
5′AATTCAAAAATGAAGGGCGAGTGAATCTAAGCTCGAGCTTAGATTCACTCGCCCT TCA 3′

Cell-line generation

10A.PE and 10A.PM cells were generated as described previously (12). For doxycycline-inducible expression of empty vector or V5-MYC, the 10A.P cell line was transfected with pLenti CMV rtTA3 (a gift from Eric Campeau; RRID:Addgene_26429) and pLenti CMV/tight V5-MYC or pLenti CMV/tight empty vector (a gift from Eric Campeau; RRID:Addgene_26433). For the doxycycline-inducible expression of short-hairpin RNAs, forward and reverse sequence oligos were cloned into Tet-pLKO-puro (a gift from Dmitri Wiederschain; RRID:Addgene_21915) and transfected into 10A.PE and 10A.PM cells stably expressing empty vector or ectopic MYC. RNaseH^{WT} was cloned from ppyCAG_RNaseH1_WT (a gift from Xiang-Dong Fu; RRID:Addgene_111906) and RNaseH^{WKKD} was cloned from ppyCAG_RNaseH1_WKKD (a gift from Xiang-Dong Fu; RRID:Addgene_111905). These constructs were cloned into pLenti CMV Blast (a gift from Eric Campeau & Paul Kaufman; RRID:Addgene_17451) for constitutive gene expression.

Genome-wide CRISPR knockout screen

The pLCKO TKOv3 pooled library (15) targets 18,053 human protein coding genes with 71,090 sgRNA sequences (4 guides/gene). In 10A.PE and 10A.PM cells, Cas9 was introduced using lentiCas9-Blast (a gift from Feng Zhang; RRID:Addgene_52962) to generate 10A.PEc and 10A.PMc cells. Both cell lines were seeded at an appropriate density to ensure 200× sgRNA library coverage of the TKOv3 library given a multiplicity of infection of 0.3, which was determined before screening. Immediately after seeding, lentivirus was added to cultures with 8 μg/mL polybrene (Sigma-Aldrich; catalog no. 107689–10G)

followed by a 24 hour incubation. Afterwards, media was changed to selection media containing 1.5 μg/mL puromycin (BioShop; catalog no. PUR333.100) to eliminate nontransduced cells over the next 48 hours. Once cells underwent puromycin selection, time zero (T0) was established and screening began. 10A.PEc and 10A.PMc cells were cultured in triplicate and passaged every 3 to 4 days for 22 days. At each passage, 20E6 cells were frozen down while a second fraction (minimum of 200× sgRNA coverage of the initial library) was cultured into fresh media. Afterwards, the Wizard Genomic DNA Purification Kit (Promega; catalog no. TM050) was used to purify genomic DNA from frozen cell pellets. Guide sequences were enriched using PCR with NEBNext Ultra II Q5 Master Mix (New England BioLabs; catalog no. M0544L). A second round of PCR was performed with i5 and i7 primers to give each condition and replicate a unique multiplexing barcode. The final PCR products were purified on 2% agarose gel, quantified, and sequenced on the Illumina HiSeq 2500 (RRID: SCR_016383) system to determine the representation of guides in each cell line.

CRISPR screen analysis

Downstream analyses were conducted using the drugZ algorithm (16), which calculates a fold-change for each sgRNA in an experimental condition (10A.PMc) relative to an untreated control (10A.PEc). A *Z*-score for each fold change is calculated using an empirical Bayes estimate of the standard deviation, by "borrowing" information from sgRNA observed at a similar frequency (read count) in the control cells. Guide-level gene scores are combined into a normalized gene-level *Z*-scores called normZ, from which *P* values are estimated from a normal distribution (16). All genes were ranked in order of their normZ scores and then used for gene set enrichment analysis (GSEA) with GO Biological Process gene sets (Broad Institute; RRID:SCR_016863) using GSEA software (Broad Institute; RRID: SCR_003199). We followed the Bader lab protocol for data analysis and visualization (17). GO processes that were significantly upregulated or downregulated were used to generate a cytoscape map (https://cytoscape.org/; RRID:SCR_003032).

EU incorporation assay

Inducible 10A.PE and 10A.PM cells were seeded at a density of 30,000 cells/well in a 12-well plate in the presence of 2 μg/mL doxycycline (Sigma-Aldrich; catalog no. D9891–25G) for 24 hour induction of empty vector or MYC. Three hours prior to harvest, negative control plates were treated with 100 μmol/L DRB (Sigma-Aldrich; catalog no. D1916–50MG) to inhibit transcription. Thirty minutes prior to harvest, wells were treated with 1 mmol/L EU (Click Chemistry Tools; catalog no. 1261–25). Cells were fixed in 3.7% paraformaldehyde (Thermo Fisher Scientific; catalog no. AC416780250) for 15 minutes at room temperature followed by permeabilization using 0.5% Triton X-100 for 15 minutes at room temperature. A Click-iT reaction (Thermo Fisher Scientific; catalog no. C10330) was then performed followed by mounting onto glass-slides using VECTASHIELD with DAPI (Vector Laboratories; catalog no. H-1200–10). Slides were imaged using the Zeiss LSM700 confocal microscope and nuclear signal intensity was analyzed using ImageJ software (https://imagej.nih.gov; RRID:SCR_003070). *P* values were calculated using one-way ANOVA with Tukey HSD *post hoc* analysis.

S9.6 and γH2AX immunofluorescence

Inducible 10A.PE and 10A.PM cells were seeded at a density of 100,000 cells/well in a six-well plate in the presence of 2 μg/mL doxycycline (Sigma-Aldrich; catalog no. D9891–25G) for the 24 hour induction of empty vector or MYC. For γH2AX experiments, cells were treated with 10 μmol/L of camptothecin (Sigma-Aldrich; catalog no. C9911–100MG) or DMSO (Sigma-Aldrich; catalog no. 472301–100ML) 1 hour before harvest. Adherent cells were briefly washed with cold PBS, fixed with 3.7% paraformaldehyde (Thermo Fisher Scientific; catalog no. AC416780250) at room temperature for 15 minutes and permeabilized for 15-minutes using 0.5% Triton X-100 (Sigma-Aldrich; catalog no. T9284–100ML). Afterwards, samples were blocked for 60 minutes at room temperature in 5% BSA and incubated with S9.6 (Kerafast; catalog no. ENH001; RRID:AB_2687463) or γH2AX (Millipore Sigma; catalog no. 05–636; RRID:AB_309864) antibody at 4°C overnight. The samples were then incubated with Alexa Fluor 488 (Thermo Fisher Scientific; A-21206; RRID:AB_2535792) for 1 hour at room temperature followed by glass coverslip mounting with VECTASHIELD with DAPI (Vector Laboratories; H-1200–10). For P493–6 suspension cells, 20,000 cells/condition were washed in cold PBS supplemented with 2% FBS (F-PBS). Cells were then resuspended in F-PBS and loaded into a Shandon Cytospin 4 Cytocentrifuge (Thermo Fisher Scientific) for mounting onto glass slides (Superfrost Plus Micro Slide, VWR, catalog no. 48311–703). Following centrifugation, cell samples were outline using a hydrophobic pen (GnomePen, FroggaBio, catalog no. BP10002). Afterwards, cells were fixed and incubated as described for adherent cell lines. Slides were imaged using the Leica SP8 confocal microscopy at a resolution of 2048×2048 pixels at ×40 magnification using oil immersion. Emission spectra excited using the 488 and 568 nm laser lines were captured using the HyD hybrid detector while DAPI fluorescence was captured using photomultiplier tubes. Image analyses for quantifying nuclear signal intensities were conducted using CellProfiler V4.2.1 (www.cellprofiler.org; RRID:SCR_007358). *P* values from the S9.6 immunofluorescence data were calculated with Student *t* test and *P* values from the γH2AX immunofluorescence data were calculated with one-way ANOVA with Tukey HSD *post hoc* analysis.

Slot blot

P493–6 cells were treated with vehicle or 0.1 μg/mL tetracycline for 48 hours to repress MYC expression. After 48 hours, 2 million cells were harvested in cell lysis buffer (10 mmol/L Tris-Cl, 10 mmol/L NaCl, 0.5% Igepal CA-630) followed by nuclear fractionation using nuclear lysis buffer (50 mmol/L Tris-Cl, 10 mmol/L EDTA, 1% SDS). Genomic DNA was extracted using 25:45:1 phenol–chloroform–isoamyl (Thermo Fisher Scientific; catalog no. 15593049) and phase-lock-gel tubes (Qiagen; catalog no. 129046). Samples were treated with RNaseH1 enzyme (NEB; catalog no. M0297S) overnight at 37°C as a specificity control. 100 ng of gDNA was loaded in duplicate in a slot blotting microfiltration device (Bio-Rad; catalog no. 1706542) onto positively charged nylon membranes (Bio-Rad; catalog no. 1620153)—one for quantifying DNA/RNA hybrids and the other for ssDNA as a loading control. Samples were incubated on the membrane for 30 minutes prior to application of a gentle vacuum. For DNA/RNA hybrids, the membrane was air dried and cross-linked with 1200J of UV light. For ssDNA samples, gDNA was denatured for 10 minutes in denaturation buffer (0.5N NaOH; 1.5M NaCl) and incubated for an additional 10 minutes in neutralization buffer (1M NaCl; 0.5M Tris-HCl pH 7.0). Afterwards, the blot was air-dried and cross-linked with 1200J of UV light. The membranes were blocked for 1 hour at room temperature using 5% milk in PBST followed by incubation with S9.6 (Kerafast; catalog no. ENH001; RRID: AB_2687463) or ssDNA (Millipore; catalog no. MAB3034; RRID: AB_11212688) antibody overnight at 4°C. IRDye secondary antibodies

(LI-COR; catalog no. 926–32211; RRID:AB_621843) were incubated for 1 hour at room temperature and blots imaged with the Odyssey Imager (LI-COR). The S9.6 signal intensities normalized to ssDNA were quantified using the ImageJ software (https://imagej.nih.gov; RRID:SCR_003070).

STRING network analysis

Interaction data for all MYC-SL R-loop factors were downloaded from the STRING database v10 using active interaction sources including text mining, experimental evidence, database annotations, co-expression, neighborhood, and co-occurrence scores (https://string-db.org; RRID:SCR_005223). Interaction scores were calculated using a high confidence threshold of ≤0.7 for the minimum required interaction score. Data were downloaded and then modified for presentation in Cytoscape 3.4.0 (https://cytoscape.org/; RRID:SCR_003032).

Clonogenic assay

10A.PE and 10A.PM cells carrying Tet-pLKO-puro (a gift from Dmitri Wiederschain; RRID:Addgene_21915) for the doxycycline-inducible expression of shLacZ, shTOP1–1 or shTOP1–2 were seeded in triplicate into a 6-well plate at a density of 100 cells/well in 2 mL of doxycycline-supplemented media at a concentration of 2 μg/mL. Colonies were permitted to grow undisturbed over 7 days, at which point, the media was removed and colonies were fixed and stained with 0.5% crystal violet staining solution or 0.5% methylene blue staining solution. *P* values were calculated using *t* tests grouped by shRNA with Holm–Bonferroni multiple-testing correction. For the stable overexpression of RNaseH1 in rescue experiments, vectors carrying wild-type or WKKD-mutant RNaseH1 (18) were cloned into pLenti CMV Blast (a gift from Eric Campeau & Paul Kaufman; RRID:Addgene_17451) and transfected into 10A.PE and 10A.PM cells carrying inducible shRNAs targeting TOP1. *P* values were calculated using *t* tests grouped by RNaseH-type and shRNA with Holm–Bonferroni multiple-testing correction.

MTT assay

10A.PE and 10A.PM cells were seeded into a 96-well plate at a density of 750 cells/well and treated with eight doses of 2-fold dilutions of camptothecin (Sigma-Aldrich; catalog no. C9911–100MG) or DMSO (Sigma-Aldrich; catalog no. 472301–100ML) vehicle control 24 hours after seeding. After 3 days, the 3-(4,5-dimethylthiazol-2-yl)-2,5-diphenyltetrazolium bromide (MTT; Sigma; catalog no. M2128–1G) reaction was performed, and absorbance was read at 570 nm on a plate reader. The dose–response curves and IC_{50} values were calculated using GraphPad Prism (v7.0; RRID:SCR_002798) or R software (V4.2.1). *P* values were calculated from extra sum-of-squares *F* test.

R-loop TCGA analysis

Pearson correlation coefficients (PCC) between the expression level of *MYC* and each of the 117 R-loop-related genes were calculated within in each TCGA dataset (RRID:SCR_003193) and then grouped to create a grouped correlation value. Two-tailed and two-sample *t* tests with significance level 0.05 were calculated when required. Correction for multiple testing was based on the FDR method. The PCCs between *MYC* and 1,000 randomly-selected equivalent gene-sets were computed to obtain null distributions. The empirical significance was obtained from assessing the observed and random PCCs.

R-loop MYC signatures analysis

PCCs between the gene expression of (i) each gene from MYC target gene signatures, TOP1, or *MYC*, and (ii) each of the 117 R-loop related genes were calculated in each TCGA study (primary tumors). The common genes between the MYC and R-loop signatures were excluded from the analyses. MYC target gene signatures included those that represented MYC upregulated (UP) and downregulated genes (DN). The analyses were performing using R software (19) and data visualization was performed using the ggplot2 package (20). For visualization, data were presented as ridgeline density plots.

Proximity ligation assay

10A.PM cells expressing ectopically expressed V5-MYC were seeded at a density of 1E5 cells/well in a 12-well tissue culture dish. Proximity ligation assay (Sigma-Aldrich; catalog no. DUO92008, DUO92002, DUO92004) was then conducted following the manufacturers protocol using mouse α-V5 (Abcam; Cat# ab27671; dilution of 1:200) and rabbit α-TOP1 (Abcam; catalog no. ab109374; dilution of 1:400). 10A.PE cells were used to assay for endogenous MYC:TOP interaction, using α-MYC (Santa Cruz Biotechnology; catalog no. sc-42; dilution of 1:200) and rabbit α-TOP1 (AbCam; catalog no. ab109374; dilution of 1:800). Images were taken using the Zeiss LSM700 confocal microscope using the 40× oil objective.

ChIP-seq, R-ChIP-seq, DRIP-seq analysis

The raw 10A.PM chromatin immunoprecipitation sequencing (ChIP)-seq data were obtained from the Gene Expression Omnibus (RRID:SCR_005012) reference GSE100335. The R software GenomicRanges package (21) was used to extract consensus sequences. Sequences of at least 1,000 bp identified in at least two of the three replicates were considered for consensus peaks. The R-loop sites were obtained from the GEO (RRID:SCR_005012) references GSE70189 (22) and GSE97072 (18). Positive and negative strand peaks were considered. The overlapping MYC and R-loop peaks were identified using the R software ChIPpeakAnno package with the findOverlapsOfPeaks function (23). The associated chromosomal regions were annotated using the assignChromosomeRegion function and human genome hg19 annotation. Permutation tests (1,000 iterations) were performed using the peakPermTest function.

Xenografts

A panel of 10A.PM cells transduced with PLKO.1 shLacZ, shTOP1–1, shTOP1–2 were subcutaneously injected into the flanks of female 6- to 8-week-old NOD-SCID mice at a concentration of 2E6 cells/100 μL containing 50% Matrigel (Corning; catalog no. 354262). Tumors were allowed to reach 100 to 200 mm^3, at which point, the animals were moved to cages with doxycycline-supplemented water (Sigma-Aldrich; catalog no. D9891–25G; 200 μg/mL). The first animal reached humane endpoint (tumor volume >1,000 mm^3) after 18 days of treatment; therefore, the rest of the animals were treated up to 18 days before tumors were harvested so that comparisons could be made across groups. Tumors were weighed and then immediately portioned for fixation and flash-freezing. Neutral-buffered formalin (Sigma-Aldrich, catalog no. HT501128; 10%) was used to fix tumors for 48 hours prior to storage in 70% ethanol at 4°C. *P* values were calculated by one-way ANOVA with Bonferroni multiple correction test. For topotecan experiments, 2E6 10A.PM cells were injected in 100 μL containing 50% Matrigel (catalog no. 354262, Corning). Tumors were allowed to reach 100 to 200 mm^3 before intraperitoneal injection with 10 mg/kg topotecan (Sigma-Aldrich; catalog no. T2705–50MG) every 8 days. The first animal reached endpoint (tumor volume >1,000 mm^3) after 28 days of treatment. The remaining animals were treated up to 28 days before tumors were harvested so that comparisons could be made across groups. *P*-value was calculated using Student *t* test. All Animal Use Protocols (AUP 972.35) describing

these experiments were approved and overseen by the Animal Resources Centre (ARC) affiliated with the University Health Network (UHN) in compliance with Canadian Council on Animal Care (CACC) guidelines.

Xenograft IHC

Formalin-fixed samples were paraffin-embedded, sectioned at 4 μmol/L thickness and stained for Ki67 (Novus; catalog no. NB110–90592). All IHC was performed as a service by the Pathology Research Program Laboratory (UHN). Pixel intensity quantification was conducted using Aperio ImageScope software (RRID: SCR_020993). *P* values calculated by one-way ANOVA with Bonferroni multiple correction test.

Analysis of MYC signatures and drug response from publicly available datasets

Gene expression data were retrieved from the 22Q2 release of the Cancer Cell Line Encyclopedia (CCLE) expression data hosted on the Cancer Dependency Map Portal (RRID:SCR_017655). The single-sample GSEA (ssGSEA) method was used from the "GSVA" package (release 3.17; ref. 24). Using gene sets from MSigDB's HALLMARK collection (including MYC_TARGETS_V1 and MYC_TARGETS_V2; RRID:SCR_016863), ssGSEA was performed on normalized RNA-seq data from 1,406 cancer cell lines. ssGSEA scores were *z*-score normalized within gene sets. Drug sensitivity was retrieved from the 19Q3 primary screen release of the PRISM drug repurposing library (25) and filtered to only include 578 cell lines that passed STR profiling. Topotecan and irinotecan data were retrieved using the compound identifiers "BRD-K55696337–003–24–4″ and "BRD-K08547377–394–03–5," respectively. In the 565 cell lines with corresponding MYC signature and drug response data, TOP1 inhibitor drug response was correlated with ssGSEA scores using Pearson correlation analyses. This analysis was repeated for cisplatin (BRD-K69172251–001–08–9), doxorubicin (BRD-K92093830–003–30–8), paclitaxel (BRD-K62008436–001–22–1), and 5′fluorouracil (BRD-K24844714–001–24–5). False discovery rate corrections were performed using the Holm–Bonferroni method.

Organoid viability assays

For organoid culturing, clear-bottomed white 384-well plates (Greiner; catalog no. 781098) were coated with 8 μL of BME (Cultrex RGF Basement Membrane Extract, Type 2, Select; Biotechne; catalog no. 3536–005–02)/well. BME was left to solidify/set for at least 20 minutes in the 37°C incubator prior to addition of the organoids. Organoids were dissociated to single cells using TrypLE (Thermo Fisher Scientific; catalog no. 12605028) and 1,500 to 3,000 cells/well were seeded in the precoated wells (described above) in 40 μL of breast organoid media containing 2% BME. Organoids were left in the incubator to grow for 3 days prior to addition of drug. Topotecan (MedChemExpress; HY-13768A) and SN-38 (MedChemExpress; S4908) stocks were prepared in DMSO and added to the organoids on Day 3 using the Tecan D300e digital drug dispenser. Samples were normalized such that all wells received the same final percentage of DMSO. After 4 days of drug treatment, cell viability was assessed using the Cell Titer-Glo 3D assay (Promega; G9683) and luminescence readings were taken using a Hidex microplate reader. All individually treated well values were normalized to the control well values. All organoid models described in this study were generated from patient tissue with written informed consent and with University Health Network Institutional Research Ethics Board (REB) approval (#14–8358; #17–5518, and #06–0196-CE). Ethics oversight was provided by the REB at the Princess Margaret Cancer Centre in compliance with the Tri-Council Policy Statement: Ethical Conduct for Research Involving Humans (Government of Canada).

Organoid RNA-seq

Organoids were recovered from BME using Organoid Harvesting Solution (BioTechne; catalog no. 3700–100–01). RNA was isolated using the NucleoSpin TriPrep Kit (Macherey-Nagel; catalog no. 740966.50). The library prep and RNA-seq was done at the Princess Margaret Genomics Centre. FASTQ files were aligned to the hg38 human reference genome using STAR 2.4.2a (26) aligner using default settings. Aligned files were then used to determine the expression levels of all transcripts RSEM 1.3.0 (27). Detailed code could be found at: https://github.com/Cesconlab/rna-seq-star-deseq2. To generate MYC signature scores of the organoids, transcripts per million (TPM) normalized RNA-seq data were analyzed using the ssGSEA method from the "GSVA" package (release 3.17; ref. 24) using MYC target gene sets from the HALLMARK collection (28).

Organoid IHC

Patient-derived breast cancer organoid samples were fixed in 10% formalin for 24 to 72 hours followed by paraffin embedding. The Y69 c-MYC antibody (ab32072, RRID:AB_731658) was used to evaluate MYC protein levels by IHC. After staining and mounting, slides were scanned using a Leica Aperio AT2 scanner (RRID:SCR_021256) at 40× objective with a resolution of 0.25 μm/pixel. For analysis, QuPath (v0.4.3; RRID:SCR_018257) software was used. The threshold for positive nuclear DAB optical density signal was 0.25 for all organoids. A minimum of 1,000 nuclei were scored representing a minimum of 50 individual organoids.

Western blotting

Subconfluent 10A.PE and 10A.PM cells expressing shRNAs against LacZ and TOP1 were induced 2 μg/mL doxycycline (Sigma-Aldrich; catalog no. D9891–25G) for 48 hours before harvest. Cell line lysates were prepared from subconfluent cells lysed in boiling SDS lysis buffer (2% SDS, 150 mmol/L NaCl, 10 mmol/L Tris-HCl pH 8.0). Fully formed organoids were recovered from BME using Cultrex Organoid Harvesting Solution (Bio-Techne; catalog no. 3700–100–01) and pelleted by centrifugation to be used for lysate preparation. Organoid pellets were frozen and lysed using 1X Laemmli buffer (2× = 125 mmol/L Tris-HCl pH 6.8, 4% SDS, 20% glycerol) supplemented with benzonase nuclease (Sigma; catalog no. E1014). Loading dye (11% glycerol, 10% β-mercaptoethanol, bromophenol blue) was added and samples were boiled for an additional 5 minutes prior to SDS-PAGE. Immunoblotting was performed against TOP1 (Abcam; catalog no. ab109374; 1:1,000, RRID: RRID:AB_10861978), MYC (9E10; homemade; 1:1000), FLAG (Sigma; catalog no. F1804–200UG; 1:1000), and actin (Sigma-Aldrich; catalog no. A2066; RRID:AB_476693; 1:2500). Primary antibodies were detected using IRDye-labeled secondary antibodies (1:20,000, LI-COR).

Statistical analysis

Statistical analyses and data visualization were performed using GraphPad Prism (v7.0) or R software (V4.2.1). Statistical significance was determined at a *P* value of <0.05 unless otherwise specified. All experiments were conducted with a minimum of three biological replicates.

Data availability

The data generated in this study are available upon request from the corresponding author. The 10A.PM ChIP, S9.6 DRIP, and R-ChIP-seq data analyzed in this study were obtained from Gene Expression

Omnibus (GEO) at GSE100335, GSE70189, and GSE97072, respectively. The human cancer patient data analyzed in this study was obtained from TCGA Research Network (https://www.cancer.gov/tcga). The gene expression data for cancer cell lines analyzed in this study were retrieved from the 22Q2 release of the CCLE expression data hosted on the Cancer Dependency Map Portal (https://depmap.org/portal/download/all/). The drug sensitivity data for cancer cell lines analyzed in this study were retrieved from the 19Q3 primary screen release of the PRISM drug repurposing library (https://depmap.org/portal/download/all/). For patient-derived organoids, the raw RNA sequencing data generated in this study for DCBPTO.66, DCBXTO.58, DCBXTO.132, and BXTO.143 are publicly available at the NCBI BioProject accession identifier PRJNA1020142. The raw sequencing data for BPTO.51 (PDO-1), BXTO.64 (PDXO-2), and BPTO.95 (PDO-3) analyzed in this study were previously published under the parenthesized aliases and obtained from https://github.com/bhklab/PDO_BME_EKGel.

Results

CRISPR-screen identifies R-loop factors as MYC-SLs

To identify MYC-SLs, we performed a genome-wide CRISPR knockout screen in the nontransformed 10A.PE and MYC-transformed 10A.PM isogenic pair (**Fig. 1A**). Cells stably expressing Cas9 were generated and validated by Western blot analysis (Supplementary Fig. S1A). The proliferation rate between the cells was indistinguishable, indicating that genes important for proliferation were expected to drop out similarly in both cell lines (Supplementary Fig. S1B). The efficacy of CRISPR-mediated editing was evaluated using a positive-control guide against *PSMD1*, an essential gene, and a random single-cutter guide targeting chromosome-10 (*RAND*) as a negative control. Cells expressing sgPSMD1 were rapidly edited, as indicated by poor proliferation over 4 days (Supplementary Fig. S1C). We transduced the TKOv3 genome-wide lentiviral library (targeting 18,053 protein-coding genes with 71,090 sgRNAs, ∼4 guides/gene; ref. 15) at a multiplicity of infection of 0.3 into both cell lines (Supplementary Fig. S1D), selected for those with a single-integrated sgRNA, and then conducted the screen (**Fig. 1B**). The cells were passaged every 3 to 4 days for a screening duration of 22 days (T22). At T22, each cell line was pooled and sequenced to characterize the abundance of barcodes associated with sgRNAs in each cell population. The total cell counts at the end of the screen for both cell lines were similar, indicating that equal coverage was maintained throughout the screens for 10A.PE and 10A.PM cells (Supplementary Fig. S1E).

To calculate the fold-change of each sgRNA between 10A.PEc and 10A.PMc at the same T22 timepoint, we used the drugZ algorithm (16). Briefly, as there were multiple sgRNAs targeting a single gene in the TKOv3 library, a *Z*-score for each sgRNA was calculated and then combined for each gene. These combined guide-level gene scores were then normalized to gene-level *Z* scores (normZ) and used to calculate *P* values and FDR. Using this method, we can directly compare the 10A.PEc and 10A.PMc cells at T22 and identify genes that differentially drop-out in 10A.PMc cells relative to the 10A.PEc cells, referring to this set as MYC-SLs.

From the CRISPR screen, MYC-SLs were identified with a normZ FDR q-value of <0.05 (Supplementary Fig. S1F). To assess whether the screen identified true MYC-SLs, we evaluated whether previously reported MYC-SLs were present in our results. We curated a gene-set representing MYC-SLs from published screens (Supplementary Table S1) and a GSEA was performed (4–11, 29). We observed an enrichment of previously reported MYC-SLs (Supplementary Fig. S1G), such as BUD31 and known regulators of transcriptional elongation (i.e., CDK7 and CDK9) that are important for MYC-driven cancers, providing confidence in the validity of the screen. To prioritize targets for validation, we ranked all genes in the screen by their normZ scores and performed a GSEA using the Gene Ontology (GO) Biological Processes (BP) gene set collection. We identified 185 GO BP sets that were significantly enriched among MYC-SLs, which were then manually grouped and labeled by their collective function (**Fig. 1C**; Supplementary Table S2).

Focusing on the largest group of gene sets that represented RNA-processing pathways, we identified many genes involved in R-loop regulation. R-loops are three-stranded nucleic acid structures that can form cotranscriptionally and when unresolved, can contribute to replication fork defects, DNA damage, and genomic instability. Exploring this, we manually-curated a gene-set including 117 proteins that have been reported to regulate or interact with R-loop structures in human cells including DNA/RNA helicases, mRNA binding/splicing factors, and topoisomerases (**Fig. 1D**; Supplementary Table S3; refs. 30–34). Using this, we performed GSEA and identified a significant enrichment of R-loop factors among the screen hits (**Fig. 1E**; Supplementary Fig. S1H). Evaluating this result for clinical relevance, we analyzed MYC and R-loop factor gene expression across The Cancer Genome Atlas (TCGA) studies (35) to assess whether they were positively correlated. For each TCGA cohort, we calculated the Pearson correlation coefficient (PCC) between MYC expression and each of the 117 R-loop factors. Significant positive PCCs between MYC and R-loop factor gene expression were identified in most human cancers (**Fig. 1F**).

The functional activity of MYC in human cancers can be evaluated using the expression data of MYC target gene signatures. To evaluate whether MYC signatures correlate with R-loop factor expression to sustain tumorigenesis, we performed Pearson correlation analyses between the expression of MYC target genes and R-loop factor expression in primary cancer datasets from TCGA (https://www.cancer.gov/tcga; Supplementary Fig. S1I). Across many established MYC target gene signatures, we observed that the expression of genes upregulated by MYC was positively correlated with R-loop factor expression.

Dysregulated MYC increases R-loop formation

As R-loops form cotranscriptionally (36), we evaluated whether dysregulated MYC increases transcriptional activity in 10A.PM cells. We performed an EU incorporation assay to evaluate nascent mRNA production following MYC or empty vector induction (Supplementary Fig. S2A). The 10A.PM cells showed significantly higher transcriptional activity than 10A.PE cells (**Fig. 2A**). Importantly, the negative control parallel samples exposed to an inhibitor of RNAPII-mediated transcription (DRB/53–85–0) showed reduced EU signal, demonstrating signal specificity.

Under conditions of elevated MYC transcriptional activity, we examined whether dysregulated MYC increases R-loop formation using S9.6 immunofluorescence. The 10A.PM cells had significantly higher nuclear signal for R-loops compared with 10A.PE cells (**Fig. 2B**). We also evaluated R-loop abundance in an independent cell system, the P493–6 lymphoblastoid model, which harbors a tetracycline-regulated MYC gene (Supplementary Fig. S2B). We observed that under MYC-high conditions, there were significantly more R-loops compared with MYC-low conditions (Supplementary Fig. S2C). Furthermore, slot-blot experiments were performed to

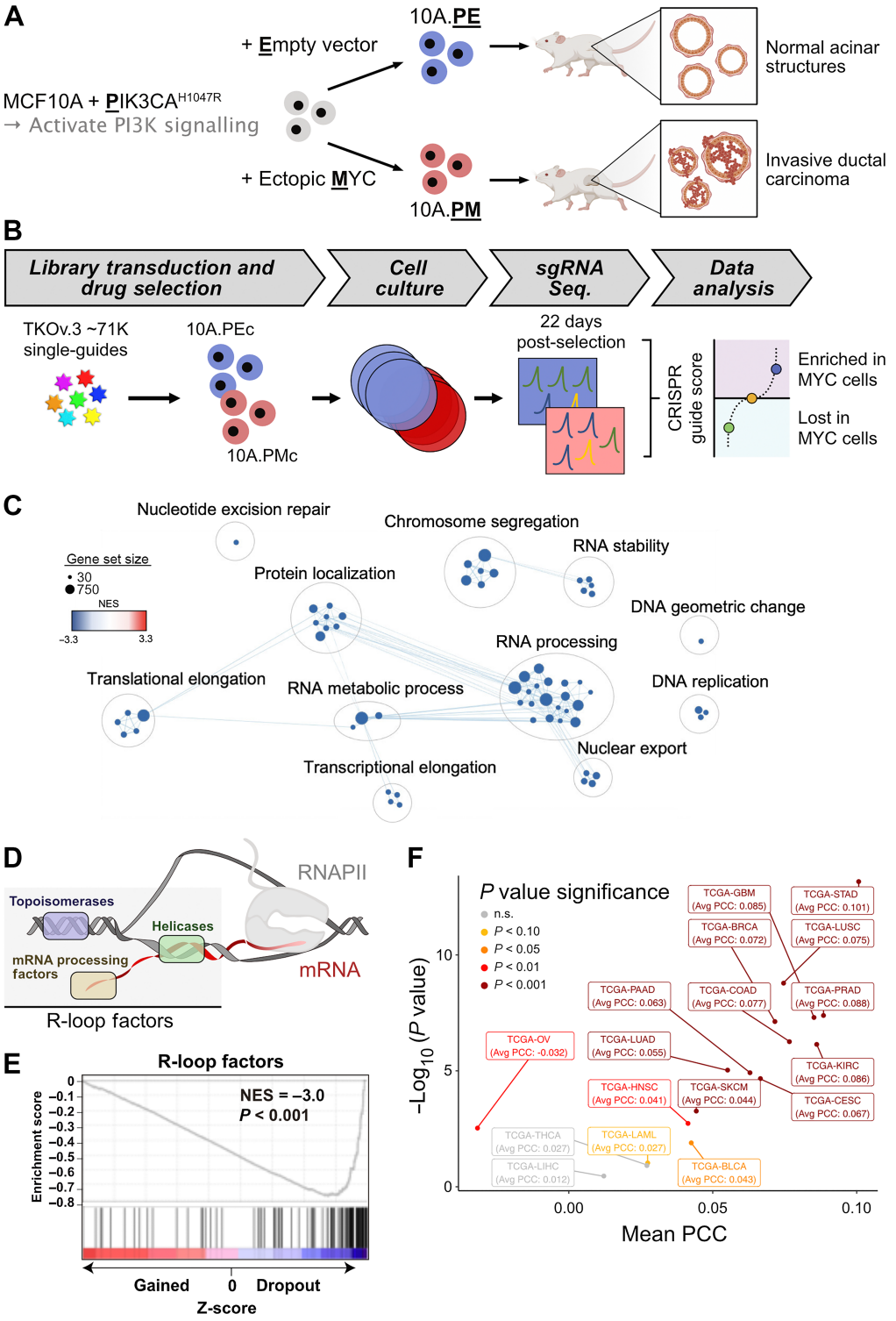

Figure 1.

CRISPR screen identifies R-loop factors as MYC-SLs. **A,** Schematic outlining the 10A.PE and 10A.PM MYC-driven and -dependent model of breast cancer. In the MCF10A cell line with an activating mutation in the *PIK3CA* gene, empty vector (10A.PE) or MYC (10A.PM) is ectopically expressed. Dysregulated MYC in 10A.PM cells initiates and sustains transformation *in vivo* (12). **B,** Pipeline of the genome-wide CRISPR knockout screen. **C,** GSEA of MYC-SL hits. Nodes represent clusters of genes with similar biological functions. Colors represent normalized enrichment scores (NES). Size indicates the number of genes per node. **D,** MYC-SLs include many proteins involved in R-loop regulation, identified as R-loop factors. **E,** GSEA identifies a significant enrichment of R-loop factors among CRISPR screen hits. The NES and corresponding *P* value are indicated. **F,** Mean PCC values between MYC gene expression and the expression of R-loop factors identified in our CRISPR screen. Data points represent PCC values in TCGA cancer cohorts. The color of the boxes represent the statistical significance of PCC values. (**A,** Created with BioRender.com.)

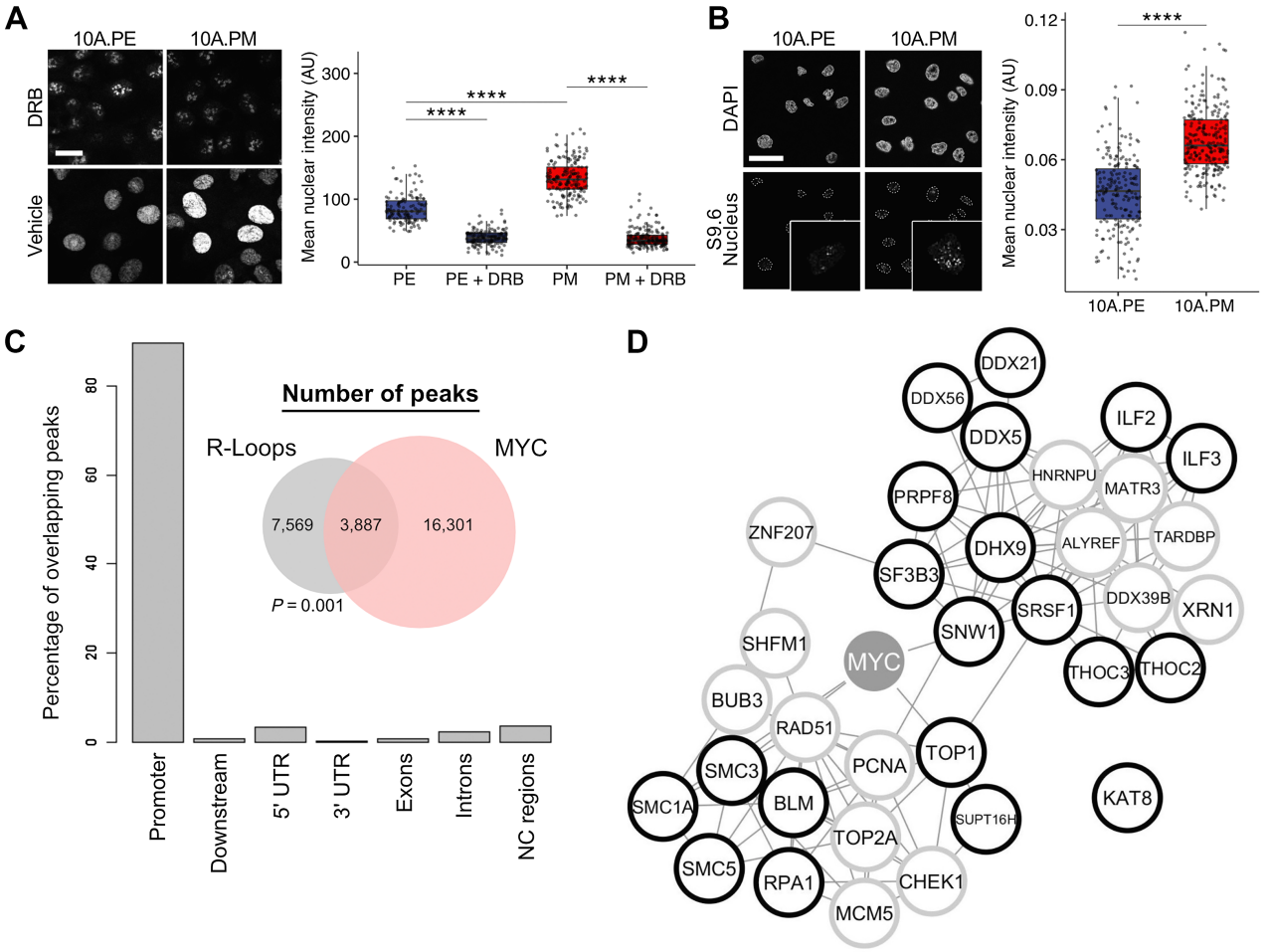

Figure 2.

Dysregulated MYC increases cotranscriptional R-loop formation. **A,** EU incorporation assay showing transcription activity following MYC induction. DRB was used as a specificity control. Representative images (left) and quantification (right) of biological replicates ($N = 3$ biological replicates) are shown. Scale bar, 20 μm. *P* values were calculated using one-way ANOVA with Tukey HSD *post hoc* test. **B,** Representative images (left) and quantification (right) of nuclear R-loops using the S9.6 immunofluorescence assay. $N = 3$ biological replicates. Scale, 40 μm. *P* values were calculated using the Student *t* test. **C,** Overlap between sites of R-loop formation and MYC-binding sites. Annotation of gene tracks identifies the genomic locations of overlapping peaks. **D,** STRING protein interaction network containing MYC-SL R-loop factors. Black border represents proteins that have been previously identified in MYC-BioID experiments as putative MYC interactors (38). ****, $P < 0.0001$.

quantify R-loop abundance. As a specificity control, parallel samples were treated with RNaseH1 enzyme. Consistently, P493–6 cells under MYC-high conditions had significantly elevated global R-loop abundance compared with MYC-low cells (Supplementary Fig. S2D).

Next, we investigated whether MYC binding sites overlap with R-loop formation. Using a MYC binding consensus sequence from ChIP-seq data in 10A.PM cells (37), we tested for overlapping R-loop peaks using publicly available R-ChIP-seq and DRIP-seq data (18, 22). We found a significant enrichment of overlapping peaks between MYC binding sites and R-loop formation from R-ChIP-seq (**Fig. 2C**; Supplementary Fig. S2E) and a DRIP-seq data (Supplementary Fig. S2F). Gene-track annotation of these overlapping peaks revealed that most of the overlap exists in promoter regions proximal to the transcriptional start sites of MYC target genes (**Fig. 2C**).

Validation of TOP1 as a MYC-SL

As MYC-SLs were enriched for R-loop factors and we showed that dysregulated MYC in the 10A.PM cells increased transcription-associated R-loops, we turned to the validation of R-loop regulators as potential MYC-SL targets. R-loop factors identified as MYC-SLs in the screen include R-loop associated helicases (DHX9, DDX5), mRNA binding/splicing factors like SRSF1, and the topoisomerases TOP1 and TOP2A (**Fig. 2D**; Supplementary Table S4). Many MYC-SL R-loop factors have also been identified as potential MYC interactors in previous MYC-BioID screens and may represent desirable targets for inhibiting MYC activity (38). TOP1 was prioritized for further validation because it has known roles in regulating R-loops at actively transcribed genes (39), is a potential MYC–protein interactor (38, 40), and has readily-available, approved inhibitors for cancer treatment, such as topotecan and irinotecan.

To evaluate TOP1 as a MYC-SL, 10A.PE and 10A.PM cells were transduced with shRNAs targeting TOP1 along with negative controls (**Fig. 3A**; Supplementary Fig. S3A), and clonogenic assays were performed. Following TOP1 knockdown, there was a significant reduction in clonogenicity in 10A.PM cells compared with 10A.PE cells (**Fig. 3B**; Supplementary Fig. S3B). As dysregulated MYC was

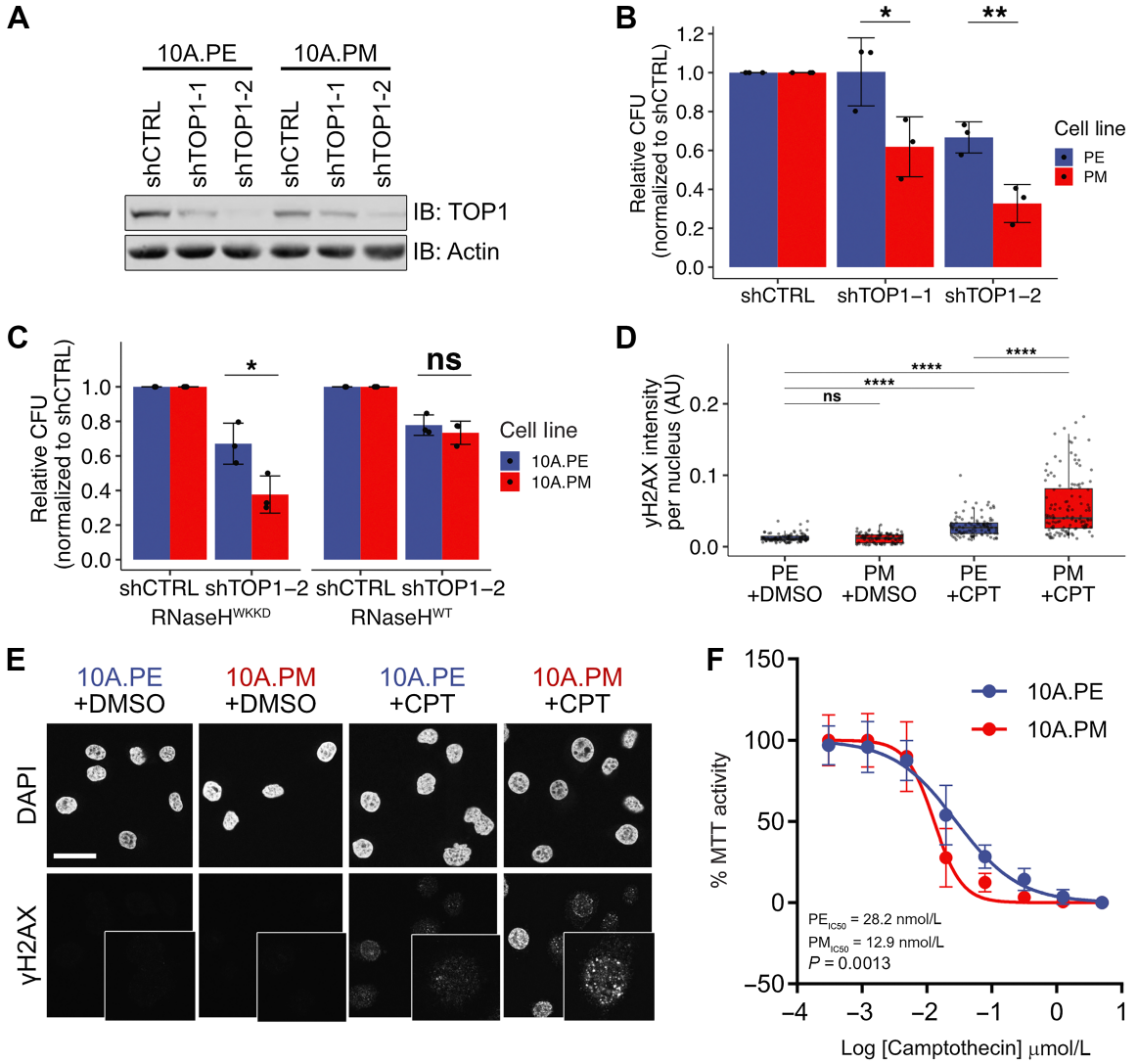

Figure 3.

Validation of TOP1 as a MYC-SL vulnerability. **A,** Western blot analysis showing TOP1 knockdown in 10A.PE and 10A.PM. **B,** Clonogenic assay using 10A.PE and 10A.PM cells with inducible shRNAs. Quantification of relative colony forming units (CFU) between groups. $N = 3$ biological experiments. Error bars, SD. *, $P < 0.05$; **, $P < 0.01$, calculated using the Student t test. **C,** Clonogenic assay using 10A.PE and 10A.PM cells with inducible shRNAs and stable overexpression of wild-type FLAG-RNaseH1^{WT} or mutant FLAG-RNaseH1^{WKKD}. Quantification of relative CFUs between groups. $N = 3$ biological experiments. Error bars, SD. *, $P < 0.05$, calculated using the Student t test. **D** and **E,** γH2AX immunofluorescence in 10A.PE and 10A.PM cells treated with DMSO or CPT. $N = 3$ biological experiments. Scale bar, 40 μm. P values were calculated using one-way ANOVA followed by Tukey HSD *post hoc* test. ****, $P < 0.0001$. **F,** Seventy-two hour MTT assay of 10A.PE and 10A.PM cells in response to a concentration-range of CPT at 1:4 dilution starting at 4 μmol/L. IC_{50} values are shown for each cell line. P values were calculated using the extra-sum-of-squares F test. $N = 3$ biological experiments. ns, nonsignificant.

demonstrated to increase R-loop levels, we evaluated whether this sensitivity to TOP1 depletion was driven by R-loop accumulation. We investigated whether expression of wild-type RNaseH1 (WT) could rescue MYC-driven sensitivity to TOP1 depletion (Supplementary Fig. S3C). As a control, we expressed a nonfunctional RNaseH1 mutant (WKKD) that does not bind nor resolve R-loops (41). We observed that overexpression of WT, but not WKKD RNaseH1 enzyme, in the setting of TOP1 depletion rescued clonogenicity specifically in 10A.PM cells (**Fig. 3C**; Supplementary Fig. S3D).

Camptothecin (CPT) is a TOP1 poison that traps TOP1 cleavage complexes on DNA to promote DNA damage. To evaluate TOP1 as a MYC-SL using a pharmacologic approach, we treated 10A.PM and 10A.PE cells with CPT and performed γH2AX immunofluorescence. We observed significantly higher nuclear intensity signal for γH2AX in 10A.PM cells compared with 10A.PE cells following CPT treatment (**Fig. 3D–E**). We also performed MTT assays to compare cell metabolic activity, a proxy for cellular viability, between 10A.PE and 10A.PM cells following CPT treatment. Consistently, 10A.PM cells were significantly more sensitive to CPT than 10A.PE cells (**Fig. 3F**). Taken together, using both genetic and pharmacologic approaches to inhibit TOP1, we confirmed TOP1 as a MYC-SL vulnerability.

As TOP1 was previously identified as a potential MYC interactor by the in-cell proximity-labeling method of BioID (38) and gene–gene

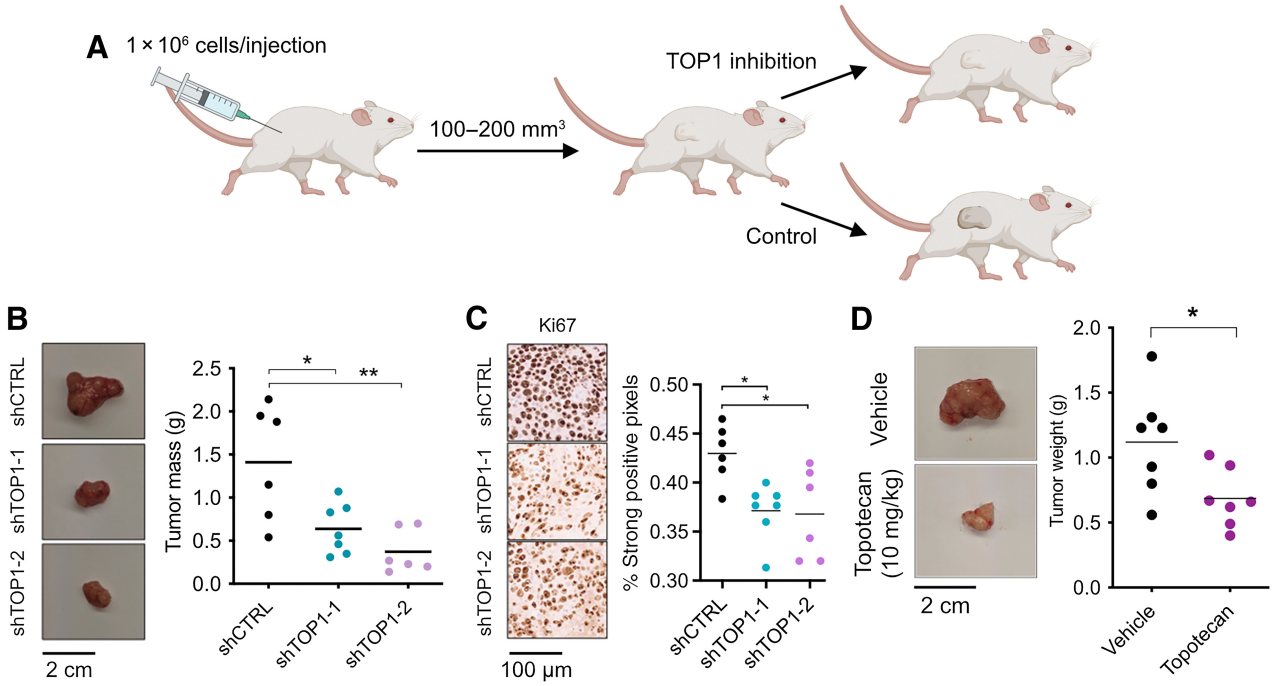

Figure 4.

TOP1 is a MYC-SL vulnerability *in vivo*. **A,** Schematic of 10A.PM xenograft experiments to evaluate effect of TOP1 inhibition on tumor growth. **B,** Tumor weights and representative images in 10A.PM xenografts following 18 days of TOP1 knockdown by shRNA compared with control shRNA. *, $P < 0.05$; **, $P < 0.01$, calculated using one-way ANOVA followed by Bonferroni multiple comparisons test. **C,** Mouse tumors were fixed, paraffin embedded, and stained for Ki67. $N = 6$ mice per treatment group except shTOP1-1, where $N = 7$. *, $P < 0.05$, calculated using one-way ANOVA followed by Bonferroni multiple comparisons test. **D,** Tumor weights from 10A.PM xenografts after topotecan treatment. Representative excised tumors shown for each treatment group. $N = 7$ mice per treatment group. *, $P < 0.05$, calculated using the Student *t* test. (**A,** Created with BioRender.com.)

interactions are more likely to be robust if their protein products interact, we also explored validation of this MYC–TOP1 interaction. Proximity-ligation assays were performed in 10A.PM cells with V5-tagged MYC. When probing for both V5 and TOP1, we observed a significant increase in nuclear intensity, providing evidence of a proximal interaction between MYC and TOP1 (Supplementary Fig. S3E). This close proximity was also confirmed with endogenous MYC in 10A.PE and MDA-MB-231 cells (Supplementary Figs. S3F and S3G).

TOP1 is a MYC-SL vulnerability *in vivo*

As the 10A.PM xenograft model has previously been shown to be MYC-driven and -dependent, we evaluated whether targeting TOP1 in this system demonstrates antitumor activity. 10A.PM shCTRL- or shTOP1-inducible cells were injected into NOD-SCID mice and tumors were allowed to reach 100 to 200 mm^3 before shRNA induction (**Fig. 4A**). After 18 days of shRNA induction, tumors expressing shCTRL formed significantly larger tumors than those expressing TOP1-targeting shRNAs (**Fig. 4B**). Furthermore, quantification of cancer cell proliferation using Ki67 IHC showed a significant decrease in shTOP1-induced tumors (**Fig. 4C**). We also assessed the efficacy of topotecan in blocking tumor growth in 10A.PM xenografts. Here, 10A.PM xenograft tumors were allowed to reach 100 to 200 mm^3 and were subsequently treated by intraperitoneal injection with topotecan or DMSO vehicle control. Consistently, topotecan inhibited tumor growth, further demonstrating that TOP1 inhibition demonstrates antitumor activity in a MYC-driven *in vivo* model of breast cancer (**Fig. 4D**).

MYC target gene signatures associate with TOP1 inhibitor response in cancer cells

To evaluate whether MYC activity is associated with TOP1 inhibitor response in publicly available datasets, we performed ssGSEA in cancer cells annotated in the CCLE. Using this method and two well-refined MYC target gene signatures from the HALLMARK collection (MYC TARGETS V1 and MYC TARGETS V2) hosted by MSigDB (28), we evaluated 1,406 cancer cell lines to score enrichment of MYC activity through the expression of its target genes (**Fig. 5A**). We then leveraged data from the PRISM Drug Repurposing screen (25) to identify the drug response profiles of 578 cancer cell lines to topotecan and irinotecan.

In the 565 cell lines with corresponding data from both datasets, we observed a significant correlation between MYC signature enrichment scores and TOP1 inhibitor drug response (**Fig. 5B**; Supplementary Fig. S4A). As many chemotherapies exploit the increased proliferative index of cancer cells, we evaluated the correlation between MYC signatures and other oncology drugs used in adjuvant or neoadjuvant breast cancer therapy, including cisplatin, doxorubicin, 5-fluorouracil, and paclitaxel. Among the approved chemotherapies, irinotecan and topotecan showed the strongest correlation with MYC activity (**Fig. 5C**; Supplementary Fig. S4B). Finally, MYC regulates many elements of cell biology through both direct and downstream regulation of its target genes, including those regulating apoptosis and metabolism. To assess whether this correlation between MYC activity and TOP1 inhibitor response is due to the enriched expression of core MYC target genes

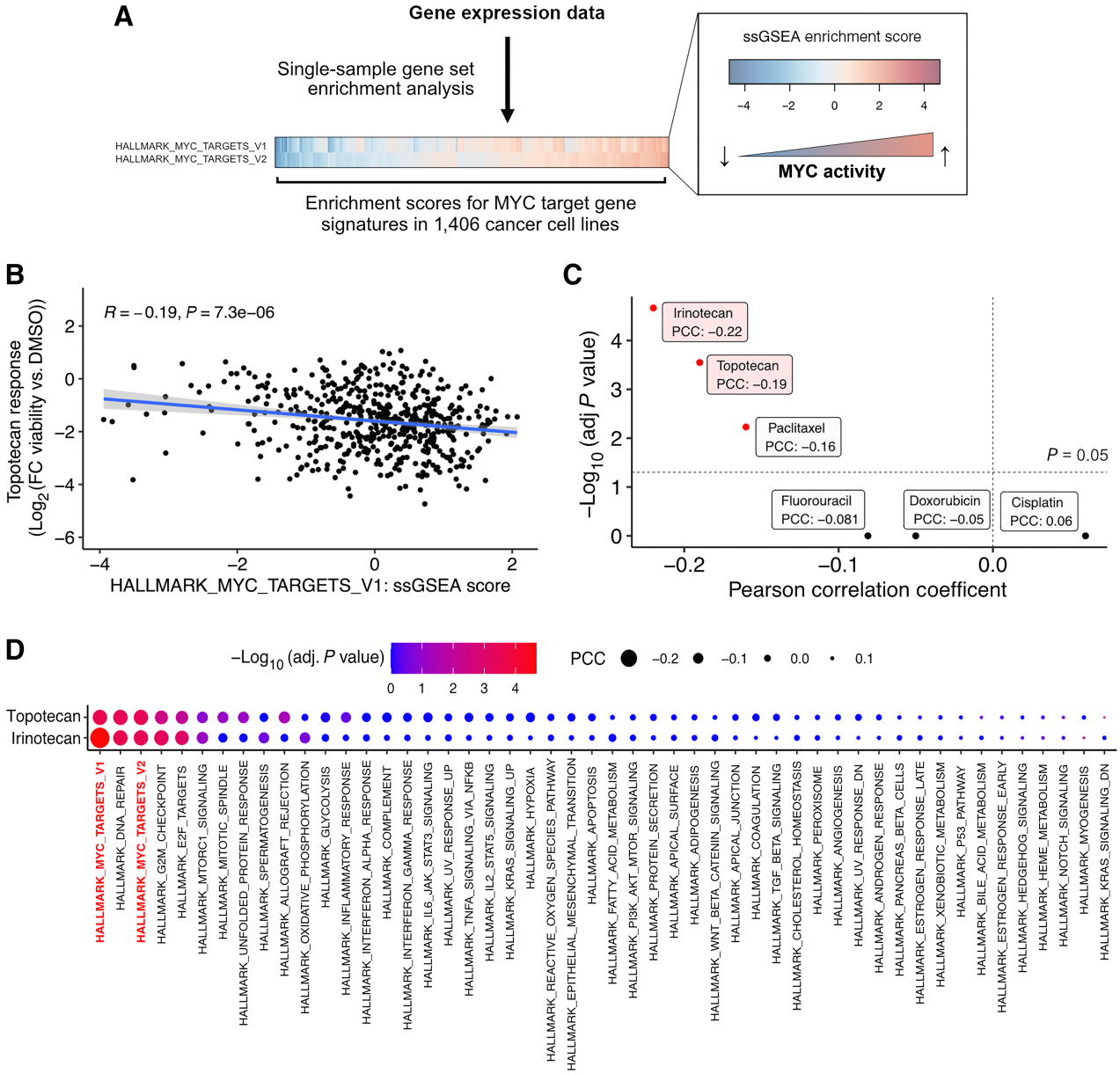

Figure 5.

MYC activity correlates with TOP1 inhibitor response in cancer cells. **A,** Schematic of pipeline to generate MYC target gene enrichment scores in 1,406 cancer cell lines annotated in the CCLE using single-sample GSEAs. Columns are sorted by aggregate row means from low to high. **B,** Pearson correlation analysis between ssGSEA scores for "HALLMARK MYC TARGETS V1" and topotecan response from the PRISM drug repurposing library. Data points represent cancer cell lines. Gray, SE of linear regression model. **C,** Pearson correlation coefficient values between drug response and MYC signature enrichment scores in cancer cell lines for each drug shown. Red, TOP1 inhibitors. *P* values were adjusted for FDR using the Holm–Bonferroni method. **D,** Bubble plot showing Pearson correlation coefficient values between ssGSEA scores for all HALLMARK gene sets and TOP1 inhibitor drug response by size. *P* values were adjusted for FDR using the Holm–Bonferroni method and visualized by color.

and not the activity of MYC-associated biological pathways, we performed ssGSEA using all 50 gene sets in the HALLMARK MSigDB collection, which collectively represent well-defined biological states or processes. In evaluating the correlation between the enrichment score of all 50 gene sets and topotecan or irinotecan response, MYC TARGETS V1 and MYC TARGETS V2 were among the top correlates with drug response (**Fig. 5D**; Supplementary Figs. S4C–S4D).

MYC activity is associated with TOP1 inhibitor response in breast cancer

To corroborate the validation data in 10A.PE/10A.PM cells and findings from publicly-available drug response data, we next evaluated a panel of breast cancer cell lines for MYC expression and response to TOP1 inhibition. Endogenous MYC protein expression was determined across the panel, which included cell lines in which *MYC* was not amplified (HCC1806, MDA-MB-231, MDA-MB-436, HCC70,

Hs578t, and MDA-MB-175VII) and three *MYC*-amplified breast cancer cell lines (SUM159PT, SKBR3, and MCF7; **Fig. 6A**; Supplementary Fig. S5A). Breast cancer models with high MYC protein levels (i.e., SUM159PT, HCC1806) were comparable with ectopic MYC levels in the 10A.PM cell model used in the CRISPR screen (Supplementary Fig. S5B). We treated this panel with eight concentrations of topotecan to generate dose–response curves and IC_{50} values (Supplementary Fig. S5C). We observed a significant correlation between MYC protein levels and topotecan response (**Fig. 6B**). The proliferative index of these cell lines was characterized by Incucyte live-cell imaging (Supplementary Fig. S5D; Supplementary Table S5). Topotecan IC_{50} values did not significantly correlate with cellular doubling time, separating cellular proliferative index from drug response (Supplementary Fig. S5E).

Patient-derived organoids (PDO) are high-fidelity models of human diseases that can be used to evaluate clinically relevant drug–response profiles. Having demonstrated that MYC protein levels were associated with topotecan response in breast cancer cells, we next evaluated topotecan and SN-38 response in a panel of breast cancer PDOs (Supplementary Fig. S6A; Supplementary Table S6). SN-38 is the active metabolite of the FDA-approved pro-drug irinotecan. Using basal RNA-seq data, we identified MYC transcripts per million (TPM) for each model, as well as ssGSEA scores for MYC TARGETS V1 and MYC TARGETS V2 (**Fig. 6C**). We observed a significant correlation between TOP1 inhibitor response and enrichment of MYC target gene signatures (**Fig. 6D**; Supplementary Fig. S6B). We evaluated relative MYC protein levels in this panel by Western blot analysis and stratified models into MYC-high or MYC-low classifications, the latter representing models with minimal detectable signal (**Fig. 6E**). The PDO models with relatively higher MYC protein expression (MYC-high) were significantly more sensitive to both topotecan and SN-38 (**Fig. 6F**). Topotecan or SN-38 IC_{50} values did not significantly correlate with PDO doubling time (Supplementary Fig. S6C). Qualitative images of representative MYC-high (BXTO.143) and MYC-low (BPTO.95) PDOs after TOP1 inhibitor treatment (i.e., topotecan or SN-38) are shown (**Fig. 6G**; Supplementary Fig. S6D). IHC staining to detect MYC protein levels showed relative MYC expression across the PDO models was consistent with Western blot analysis, providing independent assay validation (**Fig. 6H**; Supplementary Fig. S6E). Together, MYC-high breast cancer PDOs were shown to be highly responsive to topotecan and SN-38, further suggesting that TOP1 inhibition is an exploitable vulnerability in MYC-dysregulated breast cancers. Moreover, these results indicate that MYC activity could serve as a predictive biomarker for TOP1-directed therapies.

Discussion

In this study, we perform a genome-wide CRISPR knockout screen to identify novel MYC-SL targets. Here, MYC-SL targets represent proteins or processes that can be directly controlled by MYC (i.e., MYC target genes contributing to transformation), or pathways activated by the cell to support high MYC expression and transformation. Identifying such critical nodes that allow a cell to survive the consequences of MYC-driven transformation offers an opportunity to indirectly and effectively target oncogenic MYC activity. The CRISPR screen was enriched for previously identified MYC-SL vulnerabilities, providing confidence in its validity. For example, we identify important regulators of transcriptional elongation including *CDK7* and *CDK9* kinases (42, 43), as well as *BUD31*, a component of the core spliceosome and a previously validated MYC-SL gene (18). We, however, also observed an unexpected enrichment of R-loop factors among the MYC-SL hits that has not been previously reported. To the best of our knowledge, no previous MYC-SL screens have been conducted using an isogenic model in which MYC dysregulation is the oncogenic switch that drives tumor development *in vivo* and phenocopies human disease at the pathological and molecular levels. Thus, novel vulnerabilities such as R-loop factors may exist in settings that more accurately reflect MYC oncogenic function as a cancer driver. Supporting this, our analyses highlight a significant correlation between MYC gene expression and R-loop factor expression across many primary human cancer types, suggesting a role for R-loop regulation in MYC-dysregulated human cancers. Further coupling R-loop regulation with MYC transcriptional activity, we also show that known MYC target gene signatures were significantly correlated with R-loop factor expression, suggesting that MYC-associated regulation of R-loop factors via its transcriptional programs may enable MYC-driven transformation.

In exploring whether R-loop regulators can be exploited as MYC-SL vulnerabilities, we validate TOP1, a regulator of DNA topology and R-loop formation, as a novel MYC-SL target. We find that MYC-dysregulated cells are differentially sensitive to TOP1 knockdown compared with an isogenic control. Moreover, this decrease in cell-fitness could be rescued by the overexpression of wild-type but not mutant RNaseH1, supporting that this vulnerability is mediated by aberrant R-loop accumulation. Indeed, the inhibition of TOP1 has been previously demonstrated to increase R-loop accumulation through R-loop-favorable DNA unwound topologic states and persistent TOP1 cleavage complexes, resulting in the accumulation of DNA damage (44, 45). In agreement, we find that following TOP1 inhibition with camptothecin treatment, MYC-dysregulated cells harbor more DNA double-stranded breaks than control cells. TOP1 and TOP2 have recently been shown to associate with MYC functionally and proximally in a "topoisosome" complex (40), thereby coupling the regulation of MYC-driven transcription and regulation of DNA topology to maintain high transcriptional output and enable MYC-driven oncogenesis. Although TOP1 was prioritized for validation in this study, TOP2A was also a hit from the screen, providing additional evidence that targeting topoisomerase activity may be a potent vulnerability in MYC-driven cancers.

Our results suggest a model (**Fig. 7**) in which low level R-loop formation associated with gene transcription in nontransformed cells is readily resolved, even when TOP1 activity is suppressed; however, in MYC-transformed cells, the associated MYC-driven hypertranscription results in R-loop accumulation that leads to cell death in response to TOP1 inhibition. In support of this model, we show that MYC activation leads to elevated transcription activity and R-loop accumulation, which agrees with the role of increased transcription in R-loop formation and subsequent genomic instability in cancer (46). In addition, we observed a significant overlap between R-loops and MYC binding sites at promoter regions. As R-loops are known to form near promoters (47) and are associated with histone modifications characteristic of active transcription (48), including those linked to MYC activation (49), unscheduled R-loops likely accumulate during MYC-associated hypertranscription, which is in concordance with our data. Thus, our results support the model that MYC-dysregulated cancers have an increased dependence on regulators of R-loop formation to preserve genomic stability, and this vulnerability can be exploited by inhibiting TOP1.

As MYC is a master-regulator of gene transcription, one strategy to characterize MYC dysregulation is to evaluate the enrichment of

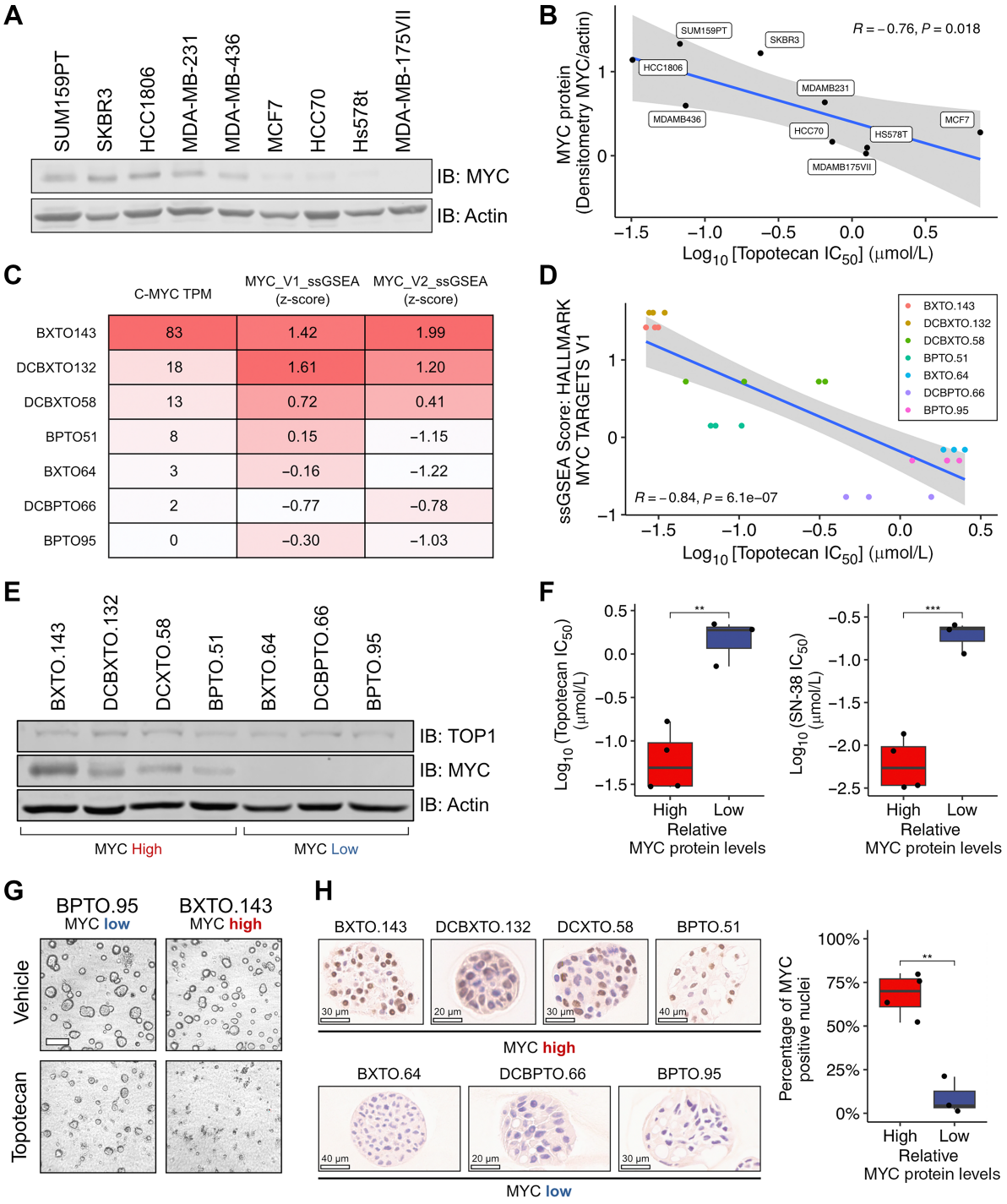

Figure 6.

Drug response to TOP1 inhibitors is MYC-driven in breast cancer. **A,** Western blot analysis showing MYC levels in a panel of breast cancer cell lines. Actin was used as a loading control. $N = 3$ biological replicates. **B,** Pearson correlation between MYC protein levels and $\log_{10}$-transformed topotecan IC_{50} values. Gray, SE of linear regression model. **C,** Heatmap showing MYC characteristics in breast cancer PDOs. Cells are pseudocolored from high (red) to low (white). **D,** Pearson correlation between MYC target gene signature enrichment scores and $\log_{10}$-transformed topotecan IC_{50} values. Biological replicates for each PDO are shown. Gray, SE of linear regression model. **E,** Western blot analysis showing MYC and TOP1 protein levels in a panel of breast cancer PDOs. Models are stratified into MYC-high and MYC-low categories based on relative detectable signal for MYC protein. **F,** $\log_{10}$-transformed topotecan and SN-38 IC_{50} values in MYC-high and MYC-low PDOs. *T* tests were performed between groups. **, $P < 0.01$; ***, $P < 0.001$. **G,** Representative images of BPTO.95 (MYC-low) and BXTO.143 (MYC-high) PDOs following 100 nmol/L of topotecan. Scale bars, 100 μm. **H,** Left, representative images of MYC immunohistochemistry signal in MYC-high and MYC-low breast cancer PDOs. Scale bar values are shown per image. Right, quantification of proportion of MYC-positive nuclei across the panel of PDOs. Student *t* test was used to determine *P* values. **, $P < 0.01$. A minimum of 1,000 nuclei from at least 50 individual organoids was scored for each model.

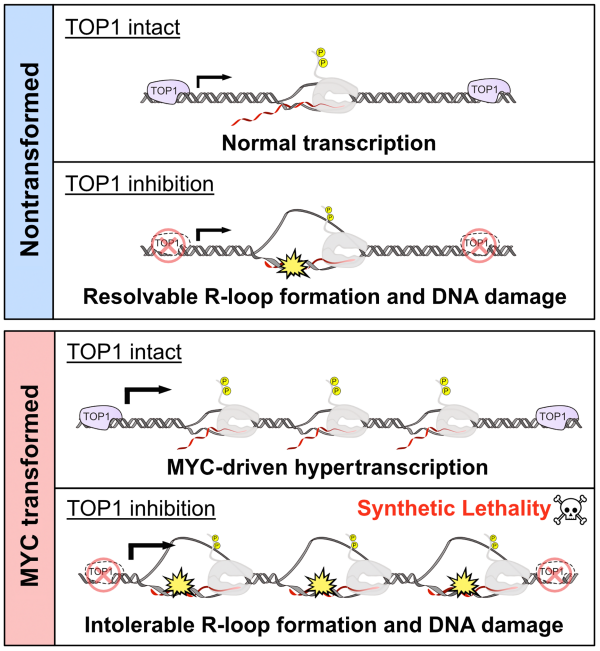

Figure 7.
Working model highlighting the proposed mechanism of TOP1 as a MYC-SL vulnerability. Under nontransformed conditions, depletion of TOP1 results in the resolvable formation of unscheduled R-loops and DNA damage. In cells under MYC-transformed conditions harboring elevated levels of transcriptional activity, TOP1 depletion leads to the intolerable accumulation of R-loops, resulting in the observed synthetic-lethal phenotype.

its target gene signatures. Two well-established gene sets describing MYC target genes include "HALLMARK MYC TARGETS V1" and "HALLMARK MYC TARGETS V2" representing 200 and 58 genes, respectively. Indeed, these gene sets have been previously shown to correlate with poor clinical outcomes in patients with breast cancer (50) and MYC protein levels (28), the latter being consistent with our results in breast cancer PDO models. Despite the large disparity in gene set size and only 18 overlapping genes, there was a general agreement between their enrichment scores in cancer models, suggesting that both signatures represent core MYC target genes capable of describing MYC activity. The significant ($|R| > 0.5$; $P < 0.05$) correlations identified between both MYC target gene signatures and the drug response profiles of two FDA-approved TOP1 inhibitors (topotecan and irinotecan) *in silico* and in breast cancer PDOs further highlight the utility of TOP1 as an actionable MYC-SL vulnerability.

Recently, topoisomerase 1 inhibitors formulated with tumor-specific antibodies in the form of antibody–drug conjugates (TOP1-ADC) have shown remarkable potential as anti-cancer therapeutics (14). Indeed, several TOP1-ADCs have been FDA-approved for the treatment of solid tumors, including breast cancer. For example, sacituzumab govitecan has been approved for use in triple-negative breast cancers, in which MYC is also one of the most frequently altered driver oncogenes. As we show that multiple models of MYC-high breast cancers, including cell line models and PDOs, are preferentially sensitive to TOP1 inhibitors, evaluation of MYC levels or activity presents an opportunity to test a predictive biomarker for these TOP1-ADCs, or to identify cancers sensitive to conventional and approved TOP1 inhibitors, which could spare the cost of ADC-related toxicities (e.g., pneumonitis) associated with these newer agents.

In conclusion, we report a strategy to target oncogenic MYC by inhibiting TOP1, a novel MYC-SL and MYC-protein interactor. These findings present an exciting opportunity to exploit TOP1, and potentially other R-loop regulators, as novel targets in MYC-dysregulated cancers. In addition, MYC levels or activity may have utility as predictive biomarkers to identify cancers sensitive to TOP1 inhibitors.

Authors' Disclosures

D.W. Cescon reports being a consultant for and on the advisory board of AstraZeneca, Exact Sciences, Eisai, Gilead, GlaxoSmithKline, Inflex, Inivata, Merck, Novartis, Pfizer, Roche, and Saga. D.W. Cescon also reports research funding to the following institutions: AstraZeneca, Guardant Health, Gilead, GlaxoSmithKline, Inivata, Knight, Merck, Pfizer, and Roche. D.W. Cescon also reports a patent (US62/675,228) for methods of treating cancers characterized by a high expression level of spindle and kinetochore associated complex subunit 3 (ska3) gene. J. Moffat reports grants from CIHR and ORF RE during the conduct of the study. No disclosures were reported by the other authors.

Authors' Contributions

P. Lin: Conceptualization, formal analysis, funding acquisition, validation, investigation, visualization, methodology, writing–original draft, writing–review and editing. **C. Lourenco:** Conceptualization, formal analysis, funding acquisition, validation, investigation, visualization, methodology, writing–review and editing. **J. Cruickshank:** Investigation, writing–review and editing. **L. Palomero:** Formal analysis, investigation, visualization, writing–review and editing. **J.E. van Leeuwen:** Investigation. **A.H. Tong:** Investigation. **K. Chan:** Investigation. **S. El Ghamrasni:** Formal analysis, writing–review and editing. **M. Pujana:** Formal analysis, funding acquisition, investigation, writing–review and editing. **D.W. Cescon:** Supervision, funding acquisition, writing–review and editing. **J. Moffat:** Writing–review and editing. **L.Z. Penn:** Conceptualization, resources, supervision, funding acquisition, project administration, writing–review and editing.

Acknowledgments

This study was funded by the Canadian Institutes of Health Research (FRN156167 to L.Z. Penn; FRN181340 to P. Lin). Funding for open access charge: Canadian Institutes of Health Research. This work was also supported by the Office of the Assistant Secretary of Defense of Health Affairs, through the Breast Cancer Research Program under Award Numbers W81XWH-21–1-0367 (to L.Z. Penn), and W81XWH-16–1-0069 (to D.W. Cescon). Opinions, interpretations, conclusions, and recommendations are those of the author and are not necessarily endorsed by the U.S. Department of Defense. This study was also partially funded by the Instituto de Salud Carlos III (PI18/01029 and PI21/01306; CIBERES) cofounded by the European Regional Development Fund (ERDF, a way to build Europe), the Generalitat de Catalunya (SGR 2017–449), and CERCA Program to IDIBELL. The authors thank members of the Penn Laboratory, Animal Resources Centre and Pathology Research Program Laboratory teams for their advice and support. The authors also thank Drs. Michael Wilson, Christopher Pearson, Wail Ba-Alawi, and Razq Hakem for their helpful discussions. Their results are partly based upon data generated by the TCGA Research Network (https://www.cancer.gov/tcga), the Cancer Cell Line Encyclopedia (CCLE; https://sites.broadinstitute.org/ccle/), and the PRISM Drug Repurposing dataset (25), and they are grateful to these consortia and coordinators for providing these data. The patient-derived breast cancer organoids were established in collaboration with the Princess Margaret Living Biobank (www.pmlivingbiobank.uhnresearch.ca). A portion of the funding for the organoid RNA-seq analysis was provided by the Princess Margaret Genomics and Epigenetics program.

The publication costs of this article were defrayed in part by the payment of publication fees. Therefore, and solely to indicate this fact, this article is hereby marked "advertisement" in accordance with 18 USC section 1734.

Note

Supplementary data for this article are available at Cancer Research Online (http://cancerres.aacrjournals.org/).

Received September 19, 2022; revised July 31, 2023; accepted October 5, 2023; published first November 21, 2023.

References

1. Lourenco C, Resetca D, Redel C, Lin P, MacDonald AS, Ciaccio R, et al. MYC protein interactors in gene transcription and cancer. Nat Rev Cancer 2021;21:579–91.
2. Felsher DW. MYC inactivation elicits oncogene addiction through both tumor cell-intrinsic and host-dependent mechanisms. Genes Cancer 2010;1:597–604.
3. Thng DKH, Toh TB, Chow EK. Capitalizing on synthetic lethality of MYC to treat cancer in the digital age. Trends Pharmacol Sci 2021;42:166–82.
4. Carroll PA, Diolaiti D, McFerrin L, Gu H, Djukovic D, Du J, et al. Deregulated Myc requires MondoA/Mlx for metabolic reprogramming and tumorigenesis. Cancer Cell 2015;27:271–85.
5. Hsu TY, Simon LM, Neill NJ, Marcotte R, Sayad A, Bland CS, et al. The spliceosome is a therapeutic vulnerability in MYC-driven cancer. Nature 2015;525:384–8.
6. Sato M, Rodriguez-Barrueco R, Yu J, Do C, Silva JM, Gautier J. MYC is a critical target of FBXW7. Oncotarget 2015;6:3292–305.
7. Zhou Z, Patel M, Ng N, Hsieh MH, Orth AP, Walker JR, et al. Identification of synthetic lethality of PRKDC in MYC-dependent human cancers by pooled shRNA screening. BMC Cancer 2014;14:944.
8. Liu L, Ulbrich J, Muller J, Wustefeld T, Aeberhard L, Kress TR, et al. Deregulated MYC expression induces dependence upon AMPK-related kinase 5. Nature 2012;483:608–12.
9. Toyoshima M, Howie HL, Imakura M, Walsh RM, Annis JE, Chang AN, et al. Functional genomics identifies therapeutic targets for MYC-driven cancer. Proc Natl Acad Sci USA 2012;109:9545–50.
10. Kessler JD, Kahle KT, Sun T, Meerbrey KL, Schlabach MR, Schmitt EM, et al. A SUMOylation-dependent transcriptional subprogram is required for Myc-driven tumorigenesis. Science 2012;335:348–53.
11. Horiuchi D, Camarda R, Zhou AY, Yau C, Momcilovic O, Balakrishnan S, et al. PIM1 kinase inhibition as a targeted therapy against triple-negative breast tumors with elevated MYC expression. Nat Med 2016;22:1321–9.
12. Lourenco C, Kalkat M, Houlahan KE, De Melo J, Longo J, Done SJ, et al. Modelling the MYC-driven normal-to-tumour switch in breast cancer. Dis Model Mech 2019;12:dmm038083.
13. Garcia-Muse T, Aguilera A. R loops: from physiological to pathological roles. Cell 2019;179:604–18.
14. Han S, Lim KS, Blackburn BJ, Yun J, Putnam CW, Bull DA, et al. The potential of topoisomerase inhibitor-based antibody-drug conjugates. Pharmaceutics 2022;14:1707.
15. Hart T, Tong AHY, Chan K, Van Leeuwen J, Seetharaman A, Aregger M, et al. Evaluation and design of genome-wide CRISPR/SpCas9 knockout screens. G3 2017;7:2719–27.
16. Colic M, Wang G, Zimmermann M, Mascall K, McLaughlin M, Bertolet L, et al. Identifying chemogenetic interactions from CRISPR screens with drugZ. Genome Med 2019;11:52.
17. Reimand J, Isserlin R, Voisin V, Kucera M, Tannus-Lopes C, Rostamianfar A, et al. Pathway enrichment analysis and visualization of omics data using g: profiler, GSEA, cytoscape and enrichmentmap. Nat Protoc 2019;14:482–517.
18. Chen L, Chen JY, Zhang X, Gu Y, Xiao R, Shao C, et al. R-ChIP using inactive RNase H reveals dynamic coupling of R-loops with transcriptional pausing at gene promoters. Mol Cell 2017;68:745–57.
19. R Development Core Team. R: A language and environment for statistical computing. Vienna, Austria: R Foundation for Statistical Computing; 2010.
20. Wickham H. ggplot2: Elegant Graphics for Data Analysis. New York: Springer-Verlag; 2016.
21. Lawrence M, Huber W, Pages H, Aboyoun P, Carlson M, Gentleman R, et al. Software for computing and annotating genomic ranges. PLoS Comput Biol 2013;9:e1003118.
22. Sanz LA, Hartono SR, Lim YW, Steyaert S, Rajpurkar A, Ginno PA, et al. Prevalent, dynamic, and conserved R-loop structures associate with specific epigenomic signatures in mammals. Mol Cell 2016;63:167–78.
23. Zhu LJ, Gazin C, Lawson ND, Pages H, Lin SM, Lapointe DS, et al. ChIPpeakAnno: a Bioconductor package to annotate ChIP-seq and ChIP-chip data. BMC Bioinf 2010;11:237.
24. Hanzelmann S, Castelo R, Guinney J. GSVA: gene set variation analysis for microarray and RNA-seq data. BMC Bioinf 2013;14:7.
25. Corsello SM, Nagari RT, Spangler RD, Rossen J, Kocak M, Bryan JG, et al. Discovering the anti-cancer potential of non-oncology drugs by systematic viability profiling. Nat Cancer 2020;1:235–48.
26. Dobin A, Davis CA, Schlesinger F, Drenkow J, Zaleski C, Jha S, et al. STAR: ultrafast universal RNA-seq aligner. Bioinformatics 2012;29:15–21.
27. Li B, Dewey CN. RSEM: accurate transcript quantification from RNA-Seq data with or without a reference genome. BMC Bioinf 2011;12:323.
28. Liberzon A, Birger C, Thorvaldsdottir H, Ghandi M, Mesirov JP, Tamayo P. The Molecular Signatures Database (MSigDB) hallmark gene set collection. Cell Syst 2015;1:417–25.
29. Marcotte R, Sayad A, Brown KR, Sanchez-Garcia F, Reimand J, Haider M, et al. Functional genomic landscape of human breast cancer drivers, vulnerabilities, and resistance. Cell 2016;164:293–309.
30. Allison DF, Wang GG. R-loops: formation, function, and relevance to cell stress. Cell Stress 2019;3:38–46.
31. Cristini A, Groh M, Kristiansen MS, Gromak N. RNA/DNA hybrid interactome identifies DXH9 as a molecular player in transcriptional termination and R-loop-associated DNA Damage. Cell Rep 2018;23:1891–905.
32. Nadel J, Athanasiadou R, Lemetre C, Wijetunga NA, Ó Broin P, Sato H, et al. RNA:DNA hybrids in the human genome have distinctive nucleotide characteristics, chromatin composition, and transcriptional relationships. Epigenetics Chromatin 2015;8:46.
33. Wang IX, Grunseich C, Fox J, Burdick J, Zhu Z, Ravazian N, et al. Human proteins that interact with RNA/DNA hybrids. Genome Res 2018;28:1405–14.
34. Santos-Pereira JM, Aguilera A. R loops: new modulators of genome dynamics and function. Nat Rev Genet 2015;16:583–97.
35. Cancer Genome Atlas Research Network, Weinstein JN, Collisson EA, Mills GB, Shaw KR, Ozenberger BA, et al. The cancer genome atlas pan-cancer analysis project. Nat Genet 2013;45:1113–20.
36. Belotserkovskii BP, Tornaletti S, D'Souza AD, Hanawalt PC. R-loop generation during transcription: formation, processing and cellular outcomes. DNA Repair (Amst) 2018;71:69–81.
37. Tu WB, Shiah YJ, Lourenco C, Mullen PJ, Dingar D, Redel C, et al. MYC interacts with the G9a histone methyltransferase to drive transcriptional repression and tumorigenesis. Cancer Cell 2018;34:579–95.
38. Kalkat M, Resetca D, Lourenco C, Chan PK, Wei Y, Shiah YJ, et al. MYC protein interactome profiling reveals functionally distinct regions that cooperate to drive tumorigenesis. Mol Cell 2018;72:836–48.
39. Manzo SG, Hartono SR, Sanz LA, Marinello J, De Biasi S, Cossarizza A, et al. DNA topoisomerase I differentially modulates R-loops across the human genome. Genome Biol 2018;19:100.
40. Das SK, Kuzin V, Cameron DP, Sanford S, Jha RK, Nie Z, et al. MYC assembles and stimulates topoisomerases 1 and 2 in a "topoisome. Mol Cell 2022;82:140–58.
41. Chen JY, Zhang X, Fu XD, Chen L. R-ChIP for genome-wide mapping of R-loops by using catalytically inactive RNASEH1. Nat Protoc 2019;14:1661–85.
42. Chipumuro E, Marco E, Christensen CL, Kwiatkowski N, Zhang T, Hatheway CM, et al. CDK7 inhibition suppresses super-enhancer-linked oncogenic transcription in MYCN-driven cancer. Cell 2014;159:1126–39.
43. Huang CH, Lujambio A, Zuber J, Tschaharganeh DF, Doran MG, Evans MJ, et al. CDK9-mediated transcription elongation is required for MYC addiction in hepatocellular carcinoma. Genes Dev 2014;28:1800–14.
44. Marinello J, Bertoncini S, Aloisi I, Cristini A, Malagoli Tagliazucchi G, Forcato M, et al. Dynamic effects of topoisomerase I inhibition on R-loops and short transcripts at active promoters. PLoS One 2016;11:e0147053.
45. Cristini A, Ricci G, Britton S, Salimbeni S, Huang SN, Marinello J, et al. Dual processing of R-loops and topoisomerase i induces transcription-dependent DNA double-strand breaks. Cell Rep 2019;28:3167–81.
46. Kotsantis P, Silva LM, Irmscher S, Jones RM, Folkes L, Gromak N, et al. Increased global transcription activity as a mechanism of replication stress in cancer. Nat Commun 2016;7:13087.
47. Chedin F. Nascent connections: R-loops and chromatin patterning. Trends Genet 2016;32:828–38.
48. Chen PB, Chen HV, Acharya D, Rando OJ, Fazzio TG. R loops regulate promoter-proximal chromatin architecture and cellular differentiation. Nat Struct Mol Biol 2015;22:999–1007.
49. Martinato F, Cesaroni M, Amati B, Guccione E. Analysis of Myc-induced histone modifications on target chromatin. PLoS One 2008;3:e3650.
50. Schulze A, Oshi M, Endo I, Takabe K. MYC targets scores are associated with cancer aggressiveness and poor survival in ER-positive primary and metastatic breast cancer. Int J Mol Sci 2020;21:8127.